frontiers | Frontiers in Earth Science

TYPE Original Research
PUBLISHED 19 January 2023
DOI 10.3389/feart.2023.1123529

OPEN ACCESS

EDITED BY
Guangjin Wang,
Kunming University of Science and Technology, China

REVIEWED BY
Guanxi Yan,
The University of Queensland, Australia
Yulong Chen,
China University of Mining and Technology, China

*CORRESPONDENCE
Shangwei Wu,
2017027@cqust.edu.cn
Jia Qin,
xizaorengui@sina.com
Xiaohua Liu,
2021207059@cqust.edu.cn

SPECIALTY SECTION
This article was submitted to Environmental Informatics and Remote Sensing, a section of the journal Frontiers in Earth Science

RECEIVED 14 December 2022
ACCEPTED 09 January 2023
PUBLISHED 19 January 2023

CITATION
Jing X, Wu S, Qin J, Li X, Liu X, Zhang Y, Mao J and Nie W (2023), Multiscale mechanical characterizations of ultrafine tailings mixed with incineration slag. *Front. Earth Sci.* 11:1123529. doi: 10.3389/feart.2023.1123529

Multiscale mechanical characterizations of ultrafine tailings mixed with incineration slag

Xiaofei Jing[1], Shangwei Wu[1]*, Jia Qin[2]*, Xiaoshuang Li[3], Xiaohua Liu[1]*, Yuanzhen Zhang[1], Jingxin Mao[1] and Wen Nie[4]

[1]School of Safety Engineering, Chongqing University of Science and Technology, Chongqing, China, [2]Chongqing Chuandongnan Survey & Design Institute Co., Ltd., Chongqing, China, [3]School of Civil Engineering, Shaoxing University, Shaoxing, China, [4]Key Laboratory of Safety and Health for Metal Mines, Maanshan, China

Adding a type of municipal solid waste (incinerator slag) into ultrafine tailings can effectively enhance the mechanical properties of tailings. With an aim to study the macro- and micro-mechanical properties of the tailings slag mixture (TSM), the strength parameters (internal friction angle, cohesion) and micro-mechanical properties with different slag contents were analyzed by geotechnical experiments and particle flow simulations, respectively. The macroscale experimental results demonstrated that the strength parameters of TSM were much higher than that of tailings. Strength parameters also showed non-linear-rising trends with increasing slag content. For the slag content of 40%, the maximum cohesiveness of TSM was determined at 65.2 kPa, and the corresponding friction angle was 39.9°C. Furthermore, the Particle Flow Code (PFC) micro-simulation software was used to analyze the micro-mechanical characteristics of the TSM at different slag contents. The microscale simulation outcomes indicated that the particle transport, particularly in their moving directions, became increasingly chaotic with an increase in the slag content; also, the slag particles significantly impacted the shear processing zone of the TSM. These experimental and numerical results brought more scientific insights into the shear failure mechanism of TSM.

KEYWORDS

ultrafine tailings, municipal solid waste, incineration slag, tailings-slag mixture (TSM), macro- and micro-mechanical characteristics

1 Introduction

In recent years, the number of ultrafine tailings reservoirs have been increasing gradually (Li et al., 2019; Shi et al., 2020; Han et al., 2022). However, the research efforts on ultrafine tailings particles are still inadequate, thereby inconducive to future sustainable development (Jing et al., 2019; Jing et al., 2021; Liu et al., 2021; Wang et al., 2022). The physical and chemical properties and engineering characteristics of slag show that slag exhibits aggregate properties. Additionally, it has many advantages, such as its high production, the massive reserve of resources, small organic content, and no radioactive harm (Huber et al., 2020). As a result, sustainable objectives, including effectively reducing slag accumulation and improving its recycling value, have become two main focuses in social research (Kumar and Singh, 2021; Joseph et al., 2022). However, the macro-mechanical properties and micro-mechanism of ultra-fine tailings particle reinforcement have not been comprehensively studied by far (Wang et al., 2020). Still, it needs to be continuously explored and further investigated in depth. Therefore,

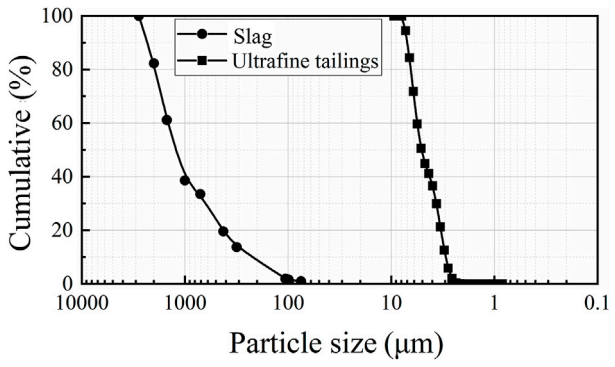

FIGURE 1
Particle size distributions of ultrafine tailings and slag particles.

characterizing the mechanical properties and failure mechanism of TSM is a pressing issue on demand of a series of urgent and compelling resolutions in geotechnical engineering.

TSM has similar structural characteristics to the soil-rock mixture (SRM). As the slag particles have a certain cohesion compared with ordinary rocks, the difference in material characteristics affects the mechanical properties of TSM. Most of the physical and mechanical properties of the SRM have been studied in three ways: laboratory testing, numerical simulation, and theoretical analysis (Chen et al., 2021; Li et al., 2022). Xing et al. (2020) used particle flow software to simulate the triaxial test numerically and elucidated the micro-mechanism of SRM with different rock content. Yin et al. (2011) used PFC discrete element particle flow to perform a micro-simulation of the triaxial test and additionally incorporated it with macroscopic mechanical properties to study the micro characteristics of hybrids. Jo et al. (2011) and Liu (2021) used PFC-2D to establish particle clusters of different shapes and the correlation between particle shape and macroscopic mechanical properties and deformation characteristics. Wang, (2017) studied the SRM through theoretical analysis, laboratory experiments, digital image processing, and PFC numerical simulation. The particle size of slag particles is different from that of ultrafine tailings, so there are similarities between TSM and SRM in terms of particle size scale differences. Therefore, the structure of TSM can refer to the structure analysis of SRM.

In this paper, the physical properties of TSM were primarily investigated. The microscopic failure deformation characteristic of TSM was subsequentially analyzed based on the observations from macroscopic experiments and microscopic numerical simulations. The microstructural variation of TSM resulting from various mixing ratios of tailings and slag particles was also studied. After collecting two experimental materials (alumina ultrafine-grained tailings from a mining area in Nanchuan, Chongqing, China, and incinerator slag from a domestic waste power plant in Chongqing), the triaxial tests were carried out on the slag-curing tailings specimens to unveil the influence of incinerator slag on the mechanical characteristics of TSM at macroscale. With the numerical simulation software of discrete element method (PFC, Itasca Inc.), the micro-mechanical properties of TSM were further studied at microscale to explore the micro-mechanics in TSM.

2 Study the shear strength characteristics of TSM

2.1 Fundamental characteristics of experimental materials

The fundamental properties of ultrafine-grained tailings and slag materials were examined independently by following the "Geotechnical Test Method Standard" (GB/T50123-2019, the Natural Standard of China). The particle size distributions of both ultrafine tailings and incinerator slag are shown in Figure 1. The standard testing outcomes are summarized in Table 1, which provides *in-situ* dry density, moisture content, and Atterberg limits for laboratory test preparation. The range of optimal moisture content of tailings reservoirs is 20%–24% (Yang and Li, 2020). In consideration of the impact of the *in-situ* tailings specimen's moisture content, the moisture content of the tailings-slag mixture specimen was adjusted to 20%, which is smaller than the moisture content of the *in-situ* tailings specimen in tailings reservoirs.

TSM and SRM both have a significant degree of structural similarity. Investigations on SRM have shown that a general coarse particle content of 30% and 70% (*via* mass fraction, mass/mass) are the two so-defined characteristics of SRM (Simoni and Houlsby, 2006); similarly, the slag contents of 0%–70% were selected in this study, as the primary research scope serving for TSM rather than SRM. The particle size distributions of the TSM in eight different slag contents (0%–70%) are shown in Figure 2. The corresponding dry densities, consolidation compression coefficients, and permeability coefficients in Table 2 were experimentally determined by following the "Geotechnical Test Method Standard" (GB/T50123-2019, the natural standard of China).

2.2 Triaxial tests

The triaxial tests in this study adopted the TSZ-2 series of automatic triaxial instruments, and the tested specimen dimensions were 61.8 mm in diameter and 125 mm in height. The drained shear tests, also known as consolidated-drained (CD), were carried out by following triaxial testing procedures to determine the physical and mechanical parameters of the tested specimens. The testing steps in detail are as follows:

(1) Preparing the triaxial specimens by mixing slag and tailings at mass ratios of 0%, 10%, 20%, 30%, 40%, 50%, 60%, and 70%, respectively; after adding slag to the tailings according to the aforementioned slag contents, then adding distilled water until the specimen moisture content reaching 20%;
(2) Checking and preparing the triaxial test instrument according to the instructions in the manual;
(3) After the installation of the specimens, saturating each tested specimen with a uniform saturation time of 1 h, followed by a Skempton B-test until the B = 0.98, also as known as the pore pressure coefficient;
(4) Three values of triaxial cell pressure, including confining pressure = 100 kPa/200 kPa/300 kPa, were selected in the controlling-acquisition interface of these triaxial tests on a computer; the mechanical tests were then initiated once the

TABLE 1 Material physics indicators.

Material	*In-situ* moisture content (%)	Maximum dry density	Liquid limits	Plastic limit
Ultrafine tailings	23	1.93 g/cm^3	44.65%	36.70%
Slag	16.8	1.61 g/cm^3	—	—

TABLE 2 Fundamental and mechanical properties of TSM in different slag contents.

Slag content (%)	0	10	20	30	40	50	60	70
Dry density (g/cm^3)	1.61	1.65	1.70	1.75	1.80	1.85	1.81	1.85
Compression coefficient a_v (MPa^{-1})	0.31	0.27	0.30	0.23	0.24	0.29	0.27	0.25
Permeability coefficient (10^{-4} cm/s)	0.09	0.15	0.18	0.17	0.21	1.63	2.02	4.23

TABLE 3 Triaxial test results.

Slag content (%)	Shear strength (kPa)			Internal friction angle φ (°)	Cohesion c (kPa)
	100	200	300		
0	245.25	460.18	655.62	30.43	12.40
10	284.50	477.33	703.16	30.77	19.70
20	455.58	789.05	1,131.20	38.91	27.80
30	600.72	972.10	1,340.93	40.48	53.30
40	690.54	908.22	1,385.60	39.90	65.20
50	798.37	1,280.10	1770.30	45.10	64.20
60	735.36	1,230.20	1738.90	45.64	47.10
70	915.60	1,119.90	1866.40	45.97	56.10

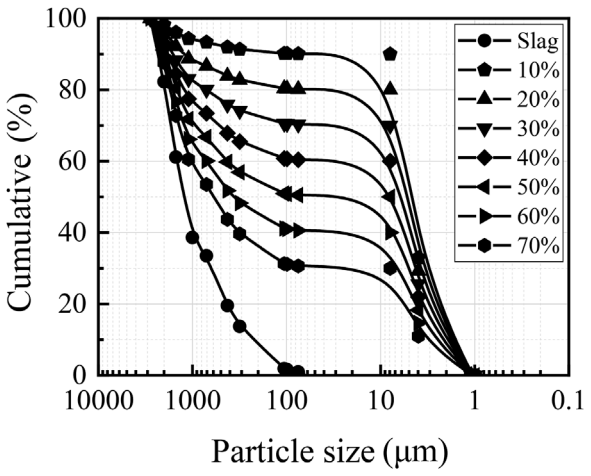

FIGURE 2
Particle size distributions of TSM with various slag content (0%–70%).

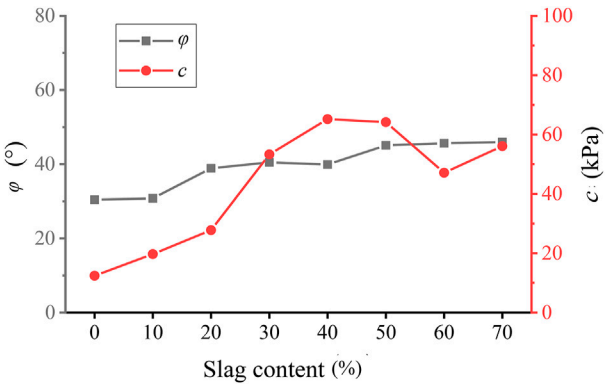

FIGURE 3
The shear strength parameters of TSM varying with slag content.

settings and parameters had been established; the strain rate of 0.08 mm/min was achieved by continuously adjusting through the operation interface until shear failure occurred;

(5) The datasets of stress and deformation were instantaneously saved in the computer from the beginning to the end of the test.

2.2.1 Triaxial test results

Table 3 shows the results of the triaxial test. The shear strength of seven TSM specimens under the previously introduced loading

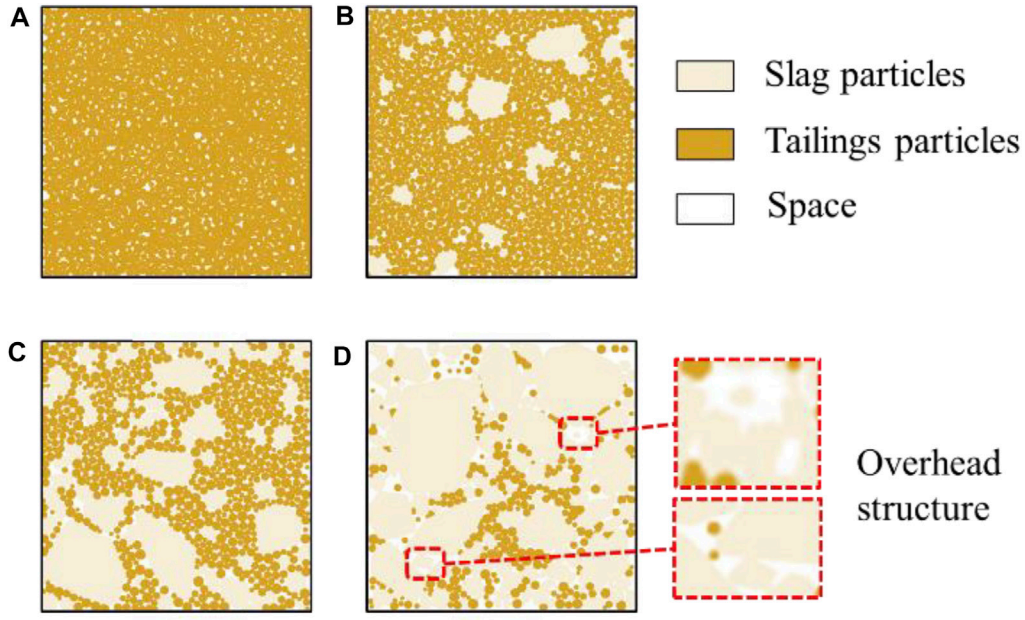

FIGURE 4
Schematic diagrams of TSM microstructure analysis.

conditions was higher than that of pure ultrafine tailings. The shear strength was increased with the increase in slag content. When the slag content reached 50%, the corresponding shear strengths under 100 kPa, 200 kPa, and 300 kPa pressure loads were 798.37 kPa, 1,280.1 kPa, and 1770.3 kPa, respectively. As for the slag content of 60%, the shear strength slightly decreased compared to the slag content of 50%. Except that the shear strength reduction was minor with increasing the slag content of TSM from 50% to 60%, it was still able to observe and elucidate that the continuous increase in slag content led to the shear strength enhancement.

Figure 3 shows that the internal friction (φ) and cohesion (c) of TSM were greater than those of pure ultrafine tailings. When the slag content was between 20% and 50%, the internal friction angle and cohesion of TSM gradually increased, while the internal friction angle and cohesion increased progressively, reaching 40%–50%. When slag content approached 60%, the cohesion suddenly dropped to 45.28 kPa. Overall, the TSM internal friction angle monotonically increased with increasing slag content. In contrast, it could not observe such a monotonic increasing relationship between the TSM cohesion and slag content, as there were two turning points at the slag contents of 40% and 60%. Despite those two turning points, the TSM cohesion could be increased by adding more slag in tailings.

Figure 4 illustrates the TSM microstructure, including the morphology, structural characteristics, and mechanical properties of both tailings and slag. According to the significant friction angle in slag, the addition of slag could influence the shear motion of TSM when the slag content was in a low range (0%–30%). As the overall TSM microstructure was more similar to the pure ultrafine tailings, the low range of slag content had less influence on the TSM cohesion (see Figure 4A, B). With increasing slag content up to 40%–50%, the ultrafine tailings and slag particles in the TSM could not contact each other to form an excellent interlocking-type microstructure, as shown in Figure 4C. Therefore, the physical and mechanical properties of the TSM should be influenced by the interparticle interactions between ultrafine tailings and slag. When the slag content exceeded 60%, the cohesion dropped sharply, and a turning point of the internal friction angle could be found. Due to the high slag content leading to the TSM microstructure mainly comprised of the slag microstructure, ultrafine tailings had minor contributions to such microstructures, as shown in Figure 4D. As a result, the tailings and slag particles were squeezed to move, consequentially forming a relatively unstable microstructure of TSM. In summary, the TSM microstructure evolvement induced by varying tailings and slag contents depended on the slag and tailings microstructures. Specifically, the coarse slag particles separated by surrounding ultrafine tailings resulted in inconsistently monotonic increases in TSM cohesion; i.e., the TSM cohesion was significantly reduced for a range of high slag content (50%–70%).

2.2.2 Analysis and comparison of shear strength characteristics

The shear strength parameters of TSM were much higher than that of pure ultrafine tailings. TSM has similar structural characteristics to the SRM. This section compares the shear strength parameters determined by the triaxial tests with the shear strength parameters obtained from the previously published literature of the relevant SRM. The internal friction angle of TSM exhibits an upward trend with the increase of slag content, similar to the experimental observations

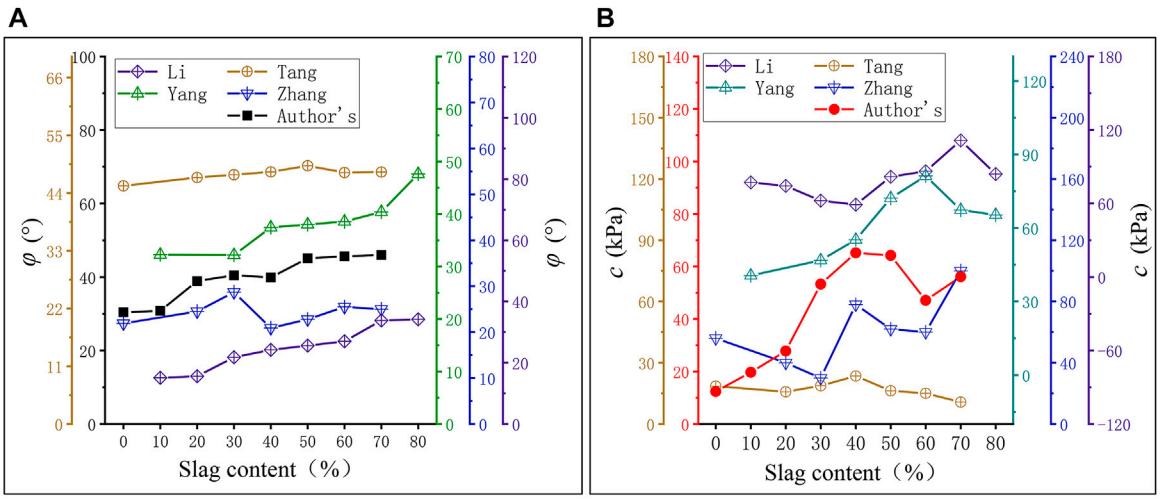

FIGURE 5
Comparison of shear strength parameters (TSM versus RSM): **(A)** The relationship between slag content and internal friction angle, **(B)** The relationship between slag content and cohesion.

reported by Tang et al. (2018), Zhang et al., 2021, and Li et al. (2007). Those observed trends are almost identical (see Figure 5A), whereas the only divergence is in the different slopes of the friction angle-slag content correlations when slag content is over 10%. It indicates that adding slag significantly affects the internal friction angle of TSM for a value of slag content higher than 10%.

The TSM cohesions measured by the triaxial tests are compared with those of the relevant SRM literature, as shown in Figure 5B. The results show that the cohesions of TSM gradually increased with increasing slag content. When the slag content is less than 40%, its strengthening tendency resembles the experimental results provided by Yang et al. (2016); When the slag content is higher than or equal to 40%, the trend seems closer to that presented by Zhang et al. (2021).

In assistance with analyzing the change of shear strength parameters compared to that of SRM, it is able to conclude that when the slag content is in a lower range (0%–20%), TSM is in a relatively dense microstructure containing limited numbers of slag particles in contact, the cohesion of TSM mainly depends on the tailings content and density, as shown in Figure 4A, B. When the slag content is in an intermediate range (30%–60%), the TSM microstructure exhibits a slag skeleton whose void spaces are filled with tailing particles (see Figure 4B, C). It also implies that those slag particles play a leading role in providing the skeleton stress during the triaxial shear test under the consolidated-drained condition. Until the triaxial loading action squeezes most fine particles out of the unstable slag skeleton, slag particles start to contact each other in order to form particle-particle interlocks. Therefore, the shear strength parameters of slag particles differ from that of the SRM due to the different material compositions and microstructural development (TSM versus SRM).

In conclusion, the inclusion of slag significantly increases the TSM shear strength, including both friction angle and cohesion, based on the experimental results presented in this study. The primary reason was that the material compositions and microstructure of slag skeleton have more decisive effects on the cohesiveness of pure ultrafine tailings in comparison to that of ordinary waste rock.

3 Manuscript formatting numerical simulation of micro-mechanical characteristics of the tailings-slag mixture

3.1 Development of numerical model by particle-discrete element method

3.1.1 Numerical models and element selection

The numerical simulation of the standard triaxial test in this research project was mainly divided into the following parts:

(1) The PFC-2D of the standard triaxial shear test was a well-developed model; the simulation settings included the left and right boundaries in modeling the flexible wall in the horizontal direction (see walls 3# and 4# in Figure 6A), the top and bottom boundaries in modeling the loading plate in the vertical direction (see the walls 1# and 2# in Figure 6A), the tested specimen in the spatial dimensions of 61.8 mm × 125 mm (diameter × length); to eliminate the impacts of friction between the walls and particles, the values of tangential contact stiffness and wall friction were set zero;
(2) In simulating the standard triaxial shear test, the left and right flexible walls (3# and 4#) were imposed by the stress boundary conditions to emulate the minimum principal stress (σ_3) in the standard triaxial test;
(3) The top and bottom loading plates (1# and 2#) were also imposed by the stress boundary conditions to emulate the mechanical loading device applying the maximum principal stress (σ_1) in the standard triaxial test.

Figure 6A shows the modeling setup of the standard triaxial test established in this study. Since the strength and stiffness of the TSM-particle skeleton were significantly more than that of the ultrafine tailings matrix, it was more applicable to employ clump clusters to model irregular slag particles for this custom-designed standard

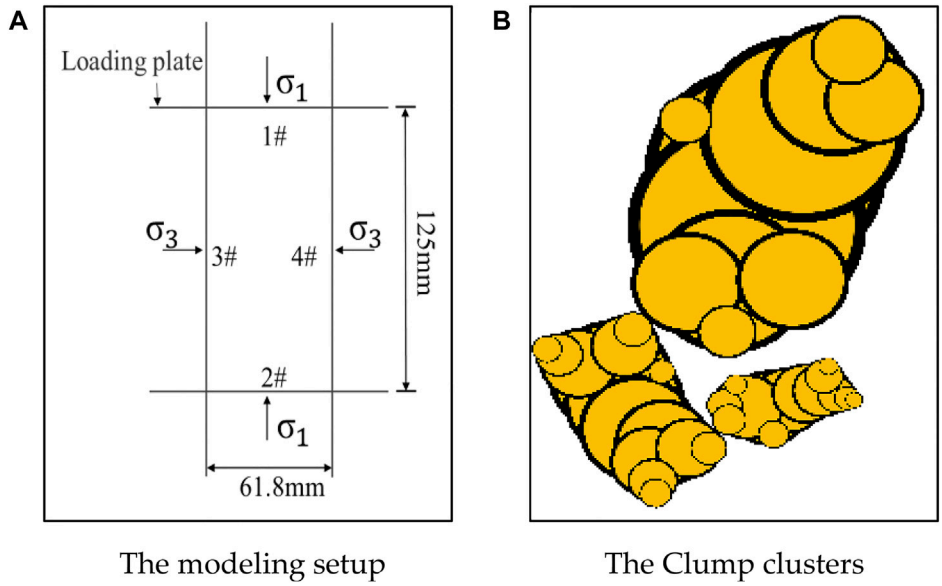

FIGURE 6
Numerical simulation model for standard triaxial tests: **(A)** The modeling setup, **(B)** The clump clusters.

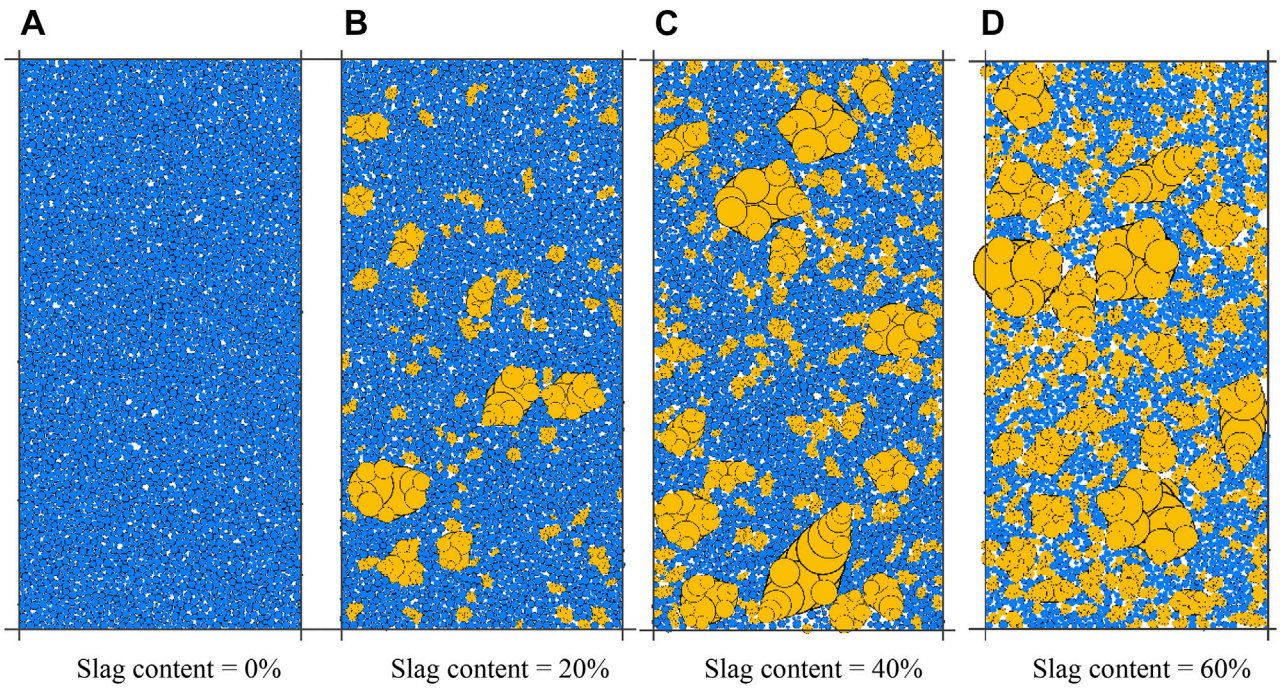

FIGURE 7
TSM specimens in different slag contents (0%–60%) generated by PFC-2D: **(A)** slag content = 0%, **(B)** slag content = 20%, **(C)** slag content = 40%, and **(D)** slag content = 60%.

triaxial simulation. Figure 6B shows an instance of the clump clusters generated in PFC-2D.

This numerical simulation adopted the same material settings and boundary and loading conditions as the standard triaxial test previously introduced (e.g., the material properties, mechanical parameters, boundary conditions, and loading rate). The modeled TSM specimens with a slag content of 0%, 20%, 40%, and 60% were digitally reconstructed based on the slag contents of the TSM specimens in the standard triaxial test. However, due to a large amount of ultra-fine particles in the simulating domain, the

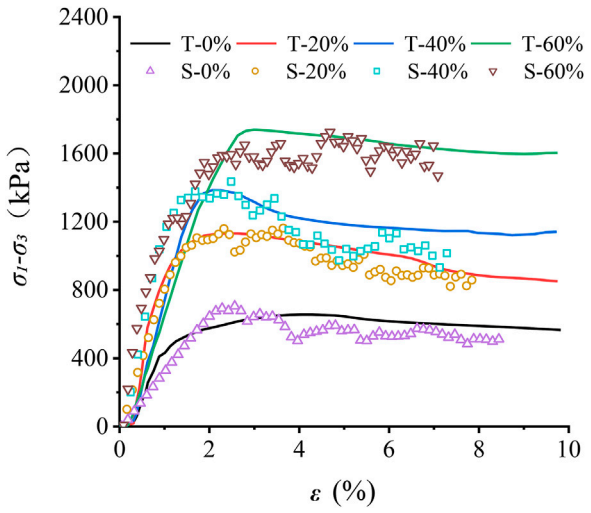

FIGURE 8
The deviator stress-strain curves of TSM specimens with four slag contents provided by the standard triaxial tests (T) and numerically simulated triaxial tests (S).

computational expense was significantly high, further leading to a relatively low computational efficiency. To overcome this issue, slag particles smaller than 0.5 mm were terminated to be generated in the simulating domain, according to the slag particle size of 0.5–1 mm in Figure 1. With this particle packing scheme available in PFC-2D (discrete element method), the particle-package models having different slag contents were eventually established, as shown in Figure 7, to study the influence of various slag contents on the mechanical properties of TSM.

3.1.2 Determination of micro-mechanical parameters for the simulated TSM specimens

For numerically modeling the TSM specimens using PFC-2D, the macroscopic mechanical behavior of the numerically simulated TSM specimens depends on the microscopic parameters, such as particle size, interparticle bonding modulus, interparticle bonding strength, interparticle bonding stiffness ratio, etc.; i.e., the microscopic parameters have significant effects on the macroscopic parameters of the mechanical constitutive relationship, including friction angle, cohesion, peak shear strength, Young's elastic modulus, Poisson's ratio, etc. (Xu and Ren, 2014; Feng et al., 2021).

In order to replicate the standard triaxial test by this newly established numerical model, the deviator stress-strain curves determined by both physical tests and numerical simulations should mutually agree well. The mechanical loading conditions, such as the vertical loading rate and confining pressure, were identically set to the discrete element numerical simulation in PFC-2D. The deviator stress-strain curves and macroscopic mechanical parameters were obtained through the standard triaxial tests (see T-labeled deviator stress-strain curves in Figure 8). Based on the experimental results, a group of micro-mechanical parameters was initially approximated for the numerical simulation of the standard triaxial test. Then, these parameters were repeatedly adjusted by following the "trial and error" method until the macroscopic mechanical characteristics of the tested TSM specimens were obtained with these approximated microscopic parameters. The most suitable micro-mechanical parameters were finally determined by continuously updating the values of these parameters after iteratively comparing the simulated outcomes with the experimental results. The fundamental and micro-mechanical parameters of the TSM specimens selected in this simulation are given in Table 4.

3.2 Analysis and discussions of numerical simulation results

3.2.1 Comparison of deviator stress-strain curve between experiment and simulation

As aforementioned, the mechanical loading conditions of the discrete element numerical simulation were identical to the loading rates and confining pressure applied in the standard triaxial tests. Therefore, to evaluate if the numerical model can effectively simulate the actual tests, the deviator stress-strain curves collected from both experimental tests and numerical simulations are henceforth compared. Also, it is convincing that the macroscopic mechanical parameters of the TSM specimens could be accurately determined when there were good agreements between experimental and numerical outcomes.

As for the simulated constraint pressure of 300 kPa, the deviator stress-strain curves outputted from experimental and numerical triaxial tests are compared in Figure 8. When the slag content was in a lower range of 0%–20%, the deviator stress continued to grow with the increase of vertical displacement indicated by strain (ε). After reaching the yielding point, the elastic deformation was followed by plastic deformation, while the deviator stress remained at a relatively constant value. The deviator stress-strain curves without apparent peak shear stress manifested the mechanical yielding followed by plastic deformation. When the slag content was in a higher range of 40%–60%, the deviator stress-strain curve mainly went through three stages: hardening, softening, and residual deformation. Specifically, those curves had apparent peak deviator stress, manifesting the transition from hardening to softening. As can be seen from Figure 8, the peak of deviator stress increased with increasing slag content. Also, the simulated curves more closely matched the deviator stress-strain relationship provided by the standard triaxial test, supporting that the numerical simulation succeeded in emulating the standard triaxial shear test under the consolidated-drain condition.

3.2.2 Analysis of mechanical characteristics

The macroscopic mechanical response of TSM with different slag contents was obtained by numerically simulating the standard triaxial tests. In addition, the deformation and shear failure mechanism of TSM and the intrinsic mechanism of the slag content's impact on its strength were also examined at microscale.

(1) Particle motion characterization:

The transporting direction of the TSM particles and the formation of the shear processing zone could be observed after outputting the vector plot of the particle velocity field for the numerical simulation of standard triaxial tests by PFC-2D. Under a confining pressure of 300 kPa, the microstructure, particle mobility, and shear processing

TABLE 4 Fundamental and mechanical parameters of the simulated TSM specimens.

Category	Density ($kg·m^{-3}$)	Coefficient of friction	Interparticle bonding stiffness (Pa)	Interparticle bonding stiffness ratio	Normal bonding strength (N)	Tangential bonding strength (N)
Tailings grain	1,580	0.5	5×10^{7}	1	1×10^{4}	1×10^{4}
Slag grain	1,210	0.75	1×10^{8}	1	1×10^{2}	1×10^{2}

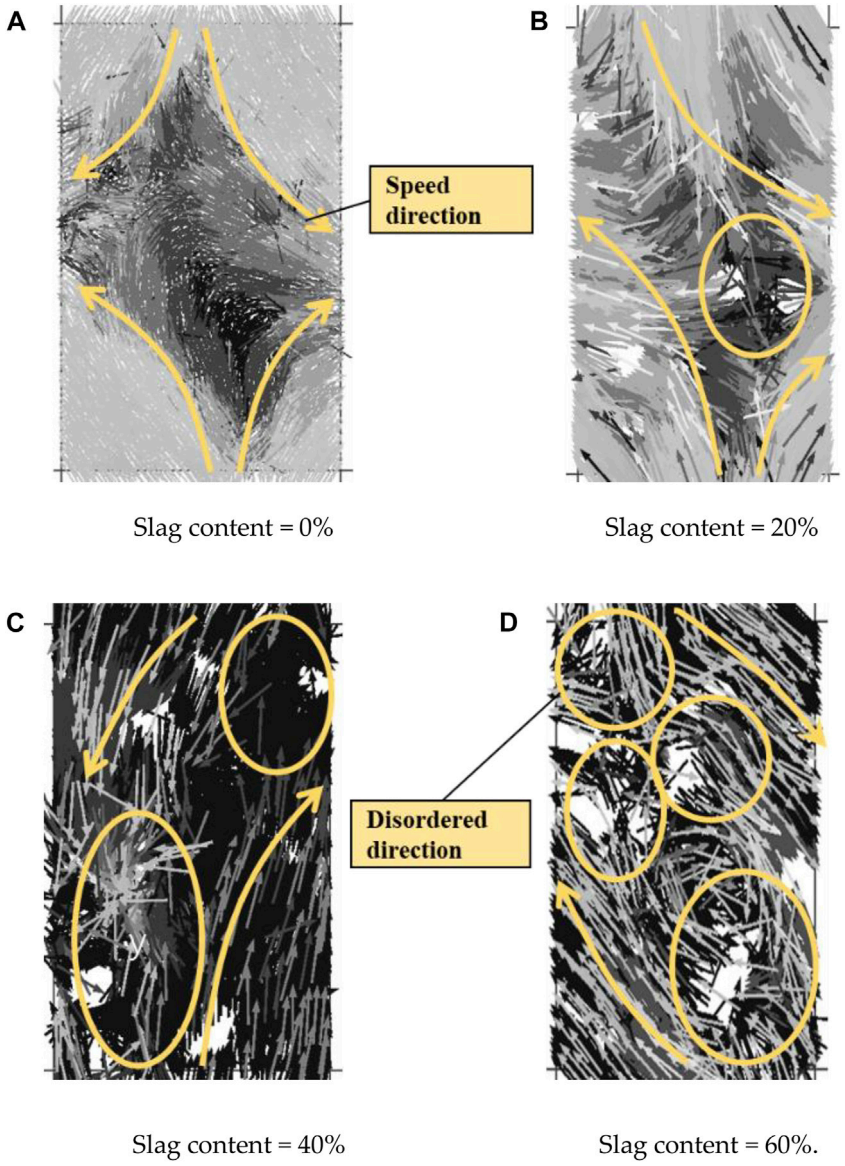

FIGURE 9
The vector plot of particle velocities for the confining pressure of 300 kPa: **(A)** slag content = 0%, **(B)** slag content = 20%, **(C)** slag content = 40%, and **(D)** slag content = 60%.

zone, which collaboratively dominated the characteristics of TSM containing 0%, 20%, 40%, and 60% slag, were examined with this simulation outcome.

The vector plot of the particle velocity field for confining pressure of 300 kPa is shown in Figure 9. The particle velocity field was plotted after completing the loading process of standard triaxial tests in simulation. The color contrast from light to dark represented the magnitude of velocity from higher to lower. The arrow in yellow color sketched the primary direction of the particle velocity. The yellow circle highlighted the disorderly portion of the particle velocity direction.

By comparing the particle velocity field of TSM specimens in different contents, it is evident that as for the slag content of 0%, the particles move from the direction of vertical load to the direction of

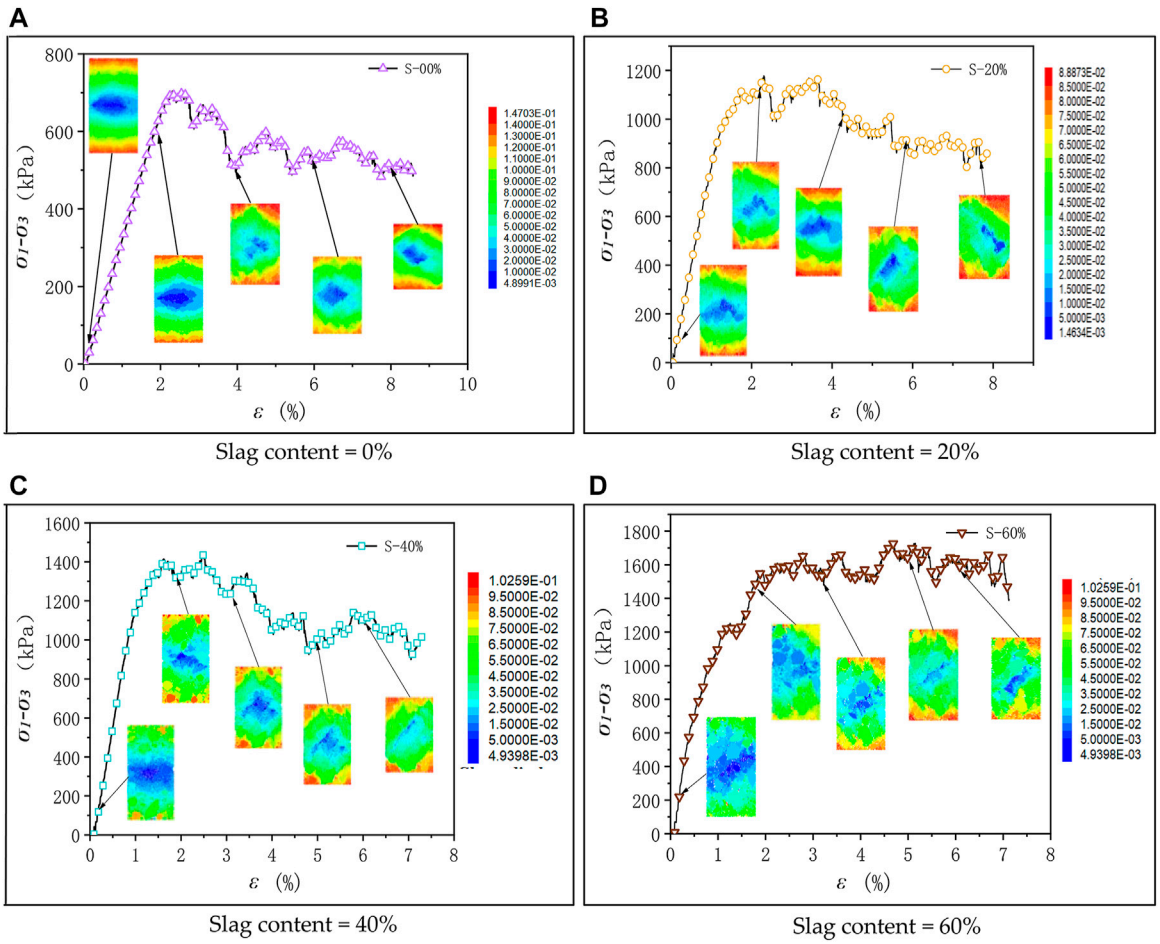

FIGURE 10
Displacement contour plots at five stages along the deviator stress-strain curves of the four TSM specimens with **(A)** slag content = 0%, **(B)** slag content = 20%, **(C)** slag content = 40%, and **(D)** slag content = 60% when the confining pressure of 300 kPa.

confining load (see Figure 9A). A few particles in the middle of the specimen were invertedly moved. The shear processing zone was not apparent, and the simulated specimen finally exhibited its deformation in the bulging form, which was similar to the final state of the deformation observed from the standard triaxial test.

While the slag content was adjusted to 20%, the particle velocity direction started to diverge due to the influence of the slag particles. As a result, the shear processing zone began to appear, for which the development of the shear processing zone was mainly affected by the velocity direction of the ultrafine tailings particles.

For the slag content reaching up to 40%, the influence of coarse particle transport on the movement of fine particles was significantly increased. The extrusion and mutual movement between particles were more prominent. The moving direction of fine particles (tailings) was mainly around the transporting tracks of coarse particles (slag). The typical movement of ultrafine tailings particles and slag particles affected the development of the shear processing zone.

When the fine content was much lower than the coarse content, as the slag content of 60% in Figure 9D, the particle transport became more chaotic, precisely in their moving directions. The coarse particles significantly impacted the development of shear processing zones in the TSM specimens.

In conclusion, in terms of the loading conditions, deforming behavior, failure mode, and deviator stress-strain relationships, the numerical simulation outcomes agreed well with the experimental results of the standard triaxial tests for the TSM specimens prepared with four different slag contents (0%–60%). Furthermore, due to the capability of observing the particle movements inside the simulated specimen, this numerical simulation has an undebatable value in analyzing the micro-mechanical characteristics of TSM.

(2) Displacement and failure characterizations:

The standard triaxial tests simulated with PFC-2D could provide the variation of particle displacements, which might be later utilized to analyze the microscopic damage inside the TSM specimens. For instance, Figure 10 demonstrates the displacement contour plots at five deforming stages along the deviator stress-strain curves of the TSM specimens having four different slag content (0%–60%) when the confining pressure was 300 kPa. In those displacement contour plots, the contouring regions assigned by dark blue denote the lowest displacement increment; in contrast, the contour regions filled with red denote the highest displacement increment.

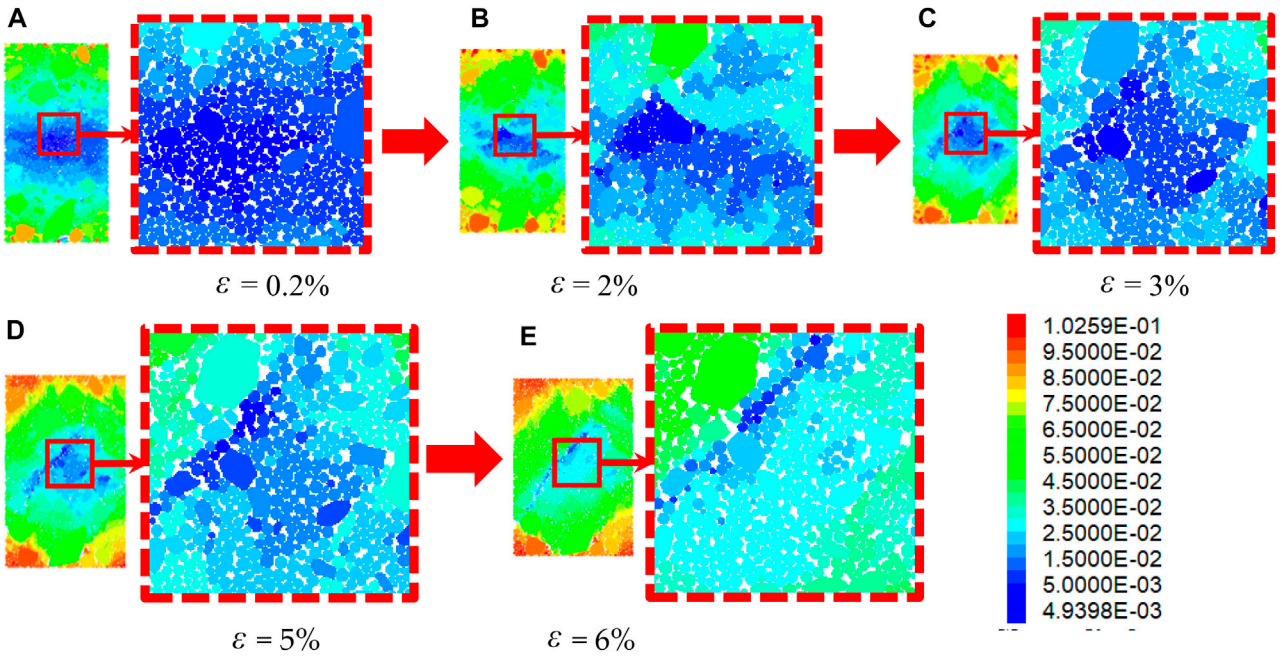

FIGURE 11
The evolution of particle displacement in the shear processing zone for the slag content of 40% at five stages: **(A)** ε = 0.2%, **(B)** ε = 2%, **(C)** ε = 3%, **(D)** ε = 5%, and **(E)** ε = 6%.

As seen in Figure 10A, since the initiation of the vertical loading to apply deviator stress, the particles nearby the boundaries of the TSM specimen began to move, and the particles centrally located in the specimen encountered minor movements. With the axial strain increasing (ε > 2%), the centrally located particles initiated distortions. When the axial strain reached around 4%, the displacement variations of those interior particles were most significant, mainly due to the stress-induced relocations of the majority of the particles. Moreover, given that the particle size of the pure tailings specimen (slag content = 0%) was uniform, the simulated specimen finally encountered the bulging failure without any apparent shear processing zone, as demonstrated by the contour plot of specimen's final displacement (ε = 8%) in Figure 10A.

By observing the displacement contour plots for the TSM specimens (slag content = 20%) in Figure 10B, particle displacements varied dramatically with the increased deviator stress. When the vertical loading began, the displacement increments of the particles inside each TSM specimen were similar to the displacement increments of the pure fine particles in Figure 10A. Such an agreement on particle displacement contour was attributable to the fact that most of the TSM particles at this stage were composed of ultrafine tailings. Thus, displacement contour plots at the first stage ($\varepsilon \leq$ 2%) in Figure 10A, B were highly similar. When the axial strain was 2%, the stress began concentrating along a potential shearing plane, and most of the particles inside the specimen had substantial displacements. Since the stress concentration area inside the TSM specimen gradually expanded, the tailing particles were partially blocked by coarse-sized slag particles. As a result, the ultrafine tailings particles were not evenly distributed inside the entire TSM specimen. The shearing processing zone was consequentially formed in the specimen, as the contour plots of ε > 5% in Figure 10B.

When the slag content of a TSM specimen was increased to 60% (see Figure 10D), the stress-induced particle redistribution at the beginning of loading ($\varepsilon \leq$ 2%) was insignificant. One possible explanation was that the TSM specimens with a high slag content had a significant amount of interior voids and a matrix consisting of slag particles. As a result, the stress was mainly distributed through the skeleton formed by the coarse-sized slag particles rather than ultrafine tailings particles. Another explanation might be that the anisotropy of the slag particles in the specimen influenced the stress concentration. During the entire loading process to apply deviator stress, the development of the shear processing zone in this TSM specimen became more apparent, implying that the specimen was more susceptible to plastic deformation predominated by shear failure.

The particle redistributing process in the TSM specimen of 40% slag content (see Figures 10C, Figure 11) was additionally compared with those of the TSM specimens of 0% and 20% slag contents (see Figure 10A, B). At the beginning of vertically compressive loading, the TSM specimen with 40% slag content had more minor particle displacements in the middle of this specimen (see Figure 11A) in comparison to the other two TSM specimens with less slag content (0% and 20%). The primary reason might be that adding slag particles into tailings increased the proportion of coarse particles in the TSM specimens. Specifically, compared to pure ultrafine particles, coarse and fine particles in such a mixture were more difficult to rotate and flip under the same loading condition provided by the deviator stress. Therefore, at the initial stage (ε = 0.2%), the vertical compression loading resulted in minimal variations of particle displacement. However, when the vertical axial strain was close to 2%, it could be observed that the specimen appeared to form stress concentration (see Figure 11B). Later, the more uniform distribution of the coarse particles in the TSM specimen with 40% slag content dispersed the

stress concentration, which was mainly reflected in the vertical axial strain of 3%, 5%, and 6%, corresponding to the displacement contour plots in Figure 11C–E.

The stress exerted on the slag particles during the stress redistribution process was anisotropic due to the different sizes and shapes of the slag particles. Hence, prominent shear processing zones appeared in the TSM specimen when continuous deviator stress was applied. Furthermore, within the duration of the vertically compressive loading process, it was evident that from the beginning stage of the formation of slag particles to the final stage of displacements of both slag particles and their surrounding tailings particles, the particle displacements in the TSM specimen initially exhibited a gradual increment and then increased significantly. Therefore, it was able to observe and conclude that when the slag content was 40%, the transition from the tailings particles originally being surrounded by slag particles to the slag particles eventually being surrounded by tailings particles consequentially led to the changes in particle displacement for the TSM specimen of 40% slag content. This phenomenon could also be explained by the fact that the TSM has the highest cohesion at a slag content of 40%, causing the most remarkable difference in peak deviator stress.

Despite the research findings above, it should be noted that this work has its natural limitations in both experiments and numerical simulations. First and foremost, the saturated condition was only considered in the triaxial tests. However, the *in-situ* might encounter a partially saturated condition, which requires technical support of unsaturated soil seepage and mechanism (Yan et al., 2022a). Second, trapping bubbles inside the pore structure can be further considered as a mechanism reducing friction between interparticle, which might lead to different research findings compared to a fully saturated condition (Ma et al., 2015; Ma et al., 2022). Last, the Darcy and non-Darcy flow as well as its corresponding flow regimes could locally exist in pore structure, so it requires further investigation of particular types of seepage flow in gravel-sized particles (Yan et al., 2022b).

4 Conclusion

Based on a literature review of the relevant research on the SRM and TSM, it is found that there have been inadequate experimental and numerical explorations of TSM in different slag content at macro- and micro-scale. Therefore, a series of standard triaxial tests were systematically carried out on TSM specimens with various slag contents (0%–60%) to investigate this research objective further. As a result, the macroscopic physical and mechanical characteristics of the TSM sample with different slag contents were obtained, as well as the effects of various slag contents on the macroscopic mechanical performance and interparticle structure of the TSM specimens. Subsequentially, the microscopic failure mechanism within the standard triaxial test and the interparticle interaction between incinerator slag and ultrafine tailings were examined by applying discrete element simulation with PFC-2D. The main conclusions obtained by experimental and numerical methods could be summarized as follows.

(1) The standard triaxial tests were used to analyze the deviator stress-strain relationships, the macroscopic deformation mechanism, and shear failure mode under a series of different testing conditions by varying slag contents and triaxial loads. The shear strengths of all selected TSM specimens were higher than that of pure ultrafine tailings. The fundamental shear strength parameters, including internal friction angle and cohesion, increased with increasing the slag content from 0% to 40%. Then, those parameters decreased slightly when the slag content was increased from 40% to 60%. The maximum cohesion was observed when the slag content was 40%. Therefore, even though the incremental resolution of slag content was 10%, the optimum slag content of 40% could be roughly estimated for engineering practice.

(2) The standard triaxial tests were modeled using the discrete element method with numerical simulation software of PFC-2D to explore the microscopic mechanism further. Referring to the deviator stress-strain curves determined by the standard triaxial tests, these numerical simulations generated curves almost overlapping with those experimental results. The shear processing zone inside the TSM specimens of various slag contents was also investigated. The micro-mechanical features were analyzed by taking advantage of the velocity vector plot and displacement contour plot provided by these simulations. With the increasing slag content in the TSM specimens, the particle movement and flipping direction became much more chaotic under the triaxial shear loading conditions. The addition of slag particles significantly impacted the development of the shear processing zone in the TSM specimen. As for the slag content of 40%, when the vertical axial strain increased, the matrix consisting of slag particles primarily encountered the most stress concentration, which was then diverged and transmitted to the surrounding tailings particles. Finally, after this stress redistribution process, the tailings and slag particles mutually interacted to present the shear failure mode with a significant shearing plane in the TSM specimen, in contrast to the budging failure mode without an apparent shearing plane inside the specimen of pure ultrafine tailings.

Data availability statement

The original contributions presented in the study are included in the article/supplementary material, further inquiries can be directed to the corresponding authors.

Author contributions

Conceptualization, SW, XL; Methodology, XJ, WN; Validation, WN; Supervision, SW; Writing—Original Draft Preparation, XL, YZ and JM, Writing—Review and Editing, XJ, JQ.

Funding

This research is funded by National Natural Science Foundation of China (Grants No. 51974051), the China Occupational Safety and Health Association (CXCY-2021-19), the Self-made Equipment Foundation of Chongqing University of Science and Technology (No. ZZSB2019013), the Graduate Innovation Program Project of Chongqing University of Science and Technology (Grants No. YKJCX2120702, YKJCX2120719, and YKJCX2120721).

Conflict of interest

Author JQ was employed by Chongqing Chuandongnan Survey & Design Institute Co., Ltd.

The remaining authors declare that the research was conducted in the absence of any commercial or financial relationships that could be construed as a potential conflict of interest.

Publisher's note

References

Chen, X., Jing, X., Cai, H., Wang, Y., and Ye, L. (2021). Hydraulic erosion rate of reinforced tailings: Laboratory investigation and prediction model. *Advances in Materials Science and Engineering*. 2021, 1–13. doi:10.1155/2021/8764862

Feng, K., Deng, H., and Sun, C. (2021). Particle flow simulation study on uniaxial compression of coal sample with prefabricated fracture. *IOP Conference Series: Earth and Environmental Science*. 859 (1), 1755–1769. doi:10.1088/1755-1315/859/1/012069

Han, C., Tan, Y., Chu, L., Song, W., and Yu, X. (2022). Flocculation and settlement characteristics of ultrafine tailings and microscopic characteristics of flocs. *Minerals* 12 (2), 221. doi:10.3390/MIN12020221

Huber, F., Korotenko, E., Šyc, M., and Fellner, J. (2020). Material and chemical composition of municipal solid waste incineration bottom ash fractions with different densities. *Journal of Material Cycles and Waste Management*. 23 (1), 394–401. doi:10.1007/s10163-020-01109-z

Jing, X., Chen, Y., Williams, D. J., Serna, M. L., and Zheng, H. (2019). Overtopping failure of a reinforced tailings dam: Laboratory investigation and forecasting model of dam failure. *Water* 11 (2), 315. doi:10.3390/w11020315

Jing, X., Pan, C., Chen, Y., Li, X., Wang, W., and Hu, X. (2021). Improvement effect of reticular glass fibers on the mechanical properties of tailings sand with the lenticle (layered sandy soil). *Water* 13 (10), 1379. doi:10.3390/W13101379

Jo, S. A., Kim, E. K., Cho, G. C., and Lee, S. W. (2011). Particle shape and crushing effects on direct shear behavior using DEM. *Soils Found.* 51 (4), 701–712. doi:10.3208/sandf.51.701

Joseph, A. M., Matthys, S., and De Belie, N. (2022). Properties of concrete with recycled aggregates giving a second life to municipal solid waste incineration bottom ash concrete. *Sustainability* 14 (8), 4679. doi:10.3390/SU14084679

Kumar, S., and Singh, D. (2021). Municipal solid waste incineration bottom ash: A competent raw material with new possibilities. *Innovative Infrastructure Solutions* 6 (4), 201. doi:10.1007/S41062-021-00567-0

Li, C., Shi, Y., Liu, P., and Guo, N. (2019). "Analysis of the sedimentation characteristics of ultrafine tailings based on an orthogonal experiment," in In 5th ISRM Young Scholars' Symposium on Rock Mechanics and International Symposium on Rock Engineering for Innovative Future, September 2019, 1–13. doi:10.1155/2019/5137092

Li, W. S., Ding, X. L., and Wu, A. Q. (2007). Study on the degree of weakening of water storage on the direct shear strength parameters of soil-stone mixture in the Three Gorges Reservoir Area. *Rock Soil Mech.* 28 (7), 1338–1342. doi:10.16285/j.rsm.2007.07.010

Li, X., Peng, J., Xie, Y., Li, Q., Zhou, T., Wang, J., et al. (2022). Influence of high-temperature treatment on strength and failure behaviors of a quartz-rich sandstone under true triaxial condition. *Lithosphere* 2022 (10), 3086647. doi:10.2113/2022/3086647

Liu, K., Cai, H., Jing, X., Chen, Y., Li, L., Wu, S., et al. (2021). Study on hydraulic incipient motion model of reinforced tailings. *Water* 13 (15), 2033. doi:10.3390/W13152033

Liu, N. (2021). Numerical simulation of foundation pit-slope based on PFC. *World Scientific Research Journal*. 7 (9), 87–96. doi:10.6911/WSRJ.202109.7(9).0013

Ma, Y., Kong, X. Z., Scheuermann, A., Galindo-Torres, S., Bringemeier, D., and Li, L. (2015). Microbubble transport in water-saturated porous media. *Water Resources Research*. 51 (6), 4359–4373. doi:10.1002/2014wr016019

Ma, Y., Yan, G., and Scheuermann, A. (2022). Discrete bubble flow in granular porous media via multiphase computational fluid dynamic simulation. *Frontiers in Earth Science*. 10, 947625. doi:10.3389/feart.2022.947625

Shi, Y., Li, C., Song, Z., and Liu, P. (2020). "Experimental study on curing of ultrafine tailings sand based on an orthogonal test," in International Conference on Ecological Resources, Energy, Construction, Transportation and Materials, Shanghai, China, December 2020. doi:10.3390/MIN1202022110

Simoni, A., and Houlsby, G. T. (2006). The direct shear strength and dilatancy of sand-gravel mixtures. *Geotechnical and Geological Engineering*. 24 (3), 523–549. doi:10.1007/s10706-004-5832-6

Tang, J., Xu, D., and Liu, H. (2018). Effect of stone content on shear characteristics of soil-stone mixture. *Rock and Soil Mechanics*. 39 (1), 93–102. doi:10.16285/j.rsm.2017.1527

Wang, P. (2017). *PFC simulation of large-scale triaxial test of soil-stone hybrid and its micro mechanical properties*. Chongqing, China: Ph.D. dissertation in Chongqing University.

Wang, G., Tian, S., Hu, B., Kong, X., and Chen, J. (2020). An experimental study on tailings deposition characteristics and variation of tailings dam saturation line. *Geomech. Eng.* 23 (1), 85–92. doi:10.12989/gae.2020.23.1.085

Wang, G., Zhao, B., Wu, B., Zhang, C., and Liu, W. (2022). Intelligent prediction of slope stability based on visual exploratory data analysis of 77 *in situ* cases. *International Journal of Mining Science and Technology*. 33 (1), 49–60. doi:10.1016/j.ijmst.2022.07.00

Xing, K., Zhou, Z., Yang, H., and Liu, B. (2020). Macro–meso freeze–thaw damage mechanism of soil–rock mixtures with different rock contents. *International Journal of Pavement Engineering*. 21 (1), 9–19. doi:10.1080/10298436.2018.1435879

Xu, L., and Ren, Q. W. (2014). Particle flow simulation of direct shear test of rock discontinuities. *Advanced Materials Research*. 1065-1069 (1065), 159–163. doi:10.4028/www.scientific.net/amr.1065-1069

Yan, G., Bore, T., Bhuyan, H., Schlaeger, S., and Scheuermann, A. (2022). The technical challenges for applying unsaturated soil sensors to conduct laboratory-scale seepage experiments. *Sensors* 22 (10), 3724. doi:10.3390/S22103724

Yan, G., Shi, H., Ma, Y., Scheuermann, A., and Li, L. (2022). Intrinsic permeabilities of transparent soil under various aqueous environmental conditions. *Géotechnique Letters*. 12 (3), 225–231. doi:10.1680/jgele.22.00049

Yang, J. H., Dong, J. Y., and Huang, Z. Q. (2016). Large-scale straight shear test study on shear strength characteristics of bulk under different rock content conditions. *Chinese Journal of Geotechnical Engineering*. 38 (2), 161–166. doi:10.11779/CJGE2016S2026

Yang, S., and Li, X. Q. (2020). Simulation analysis of large-scale straight shear test of soil-stone mixture based on 3D discrete element particle flow. *Engineering Science and Technology*. 52 (3), 78–85. doi:10.15961/j.jsuese.201900111

Yin, Y. C., Zhao, T. B., Tan, Y. L., and Zang, C. W. (2011). Particle flow simulation of rock uniaxial compression process. *Applied Mechanics and Materials*. 90-93, 497–500. doi:10.4028/www.scientific.net/amm.90-93.497

Zhang, Z. P., Fu, X. D., and Sheng, Q. (2021). Nonlinear failure strength criterion of soil-stone mixture based on rock content index. *Chinese Journal of Rock Mechanics and Engineering*. 40 (8), 1–15. doi:10.13722/j.cnki.jrme.2020.0854